This is a pre print version of the following article:

Biological and physical modification of carbonate system parameters along the salinity gradient in shallow hypersaline solar salterns in Trapani, Italy / Isaji, Y., Kawahata, H., Kuroda, J., Yoshimura, T., Ogawa, N.O., Suzuki, A., Shibuya, T., Jiménez-Espejo, F.J., Lugli, S., Santulli, A., Manzi, V., Roveri, M., Ohkouchi, N.. - In: GEOCHIMICA ET COSMOCHIMICA ACTA. - ISSN 0016-7037. - 208:(2017), pp. 354-367. [10.1016/j.gca.2017.04.013]

Terms of use:

The terms and conditions for the reuse of this version of the manuscript are specified in the publishing policy. For all terms of use and more information see the publisher's website.

14/11/2026 18:52

(Article begins on next page)

Title

Biological and physical modification of carbonate system parameters along the salinity gradient in shallow hypersaline solar salterns in Trapani, Italy

Authors and affiliations

Yuta Isaji[1]*, Hodaka Kawahata[1], Junichiro Kuroda[1], Toshihiro Yoshimura[1], Nanako O. Ogawa[2], Atsushi Suzuki[3], Takazo Shibuya[4], Francisco J. Jiménez-Espejo[2], Stefano Lugli[5], Andrea Santulli[6], Vinicio Manzi[7], Marco Roveri[7], Naohiko Ohkouchi[2]

[1]Atmosphere and Ocean Research Institute, University of Tokyo, 5-1-5 Kashiwanoha, Kashiwa, Chiba 277-8564, Japan (isaji@aori.u-tokyo.ac.jp, kawahata@aori.u-tokyo.ac.jp, kuroda@aori.u-tokyo.ac.jp, yoshimura@)aori.u-tokyo.ac.jp)

[2]Department of Biogeochemistry, Japan Agency for Marine-Earth Science and Technology (JAMSTEC), 2-15 Natsushima, Yokosuka 237-0061, Japan (nanaogawa@ jamstec.go.jp, fjjspejo@ jamstec.go.jp, nohkouchi@ jamstec.go.jp)

[3]Geological Survey of Japan, National Institute of Advanced Industrial Science and Technology (AIST), Tsukuba Central 7, 1-1-1 Higashi, Tsukuba, Ibaraki 305-8567,

Japan (a.suzuki@aist.go.jp)

[4]Department of Subsurface Geobiological Analysis and Research, Japan Agency for Marine-Earth Science and Technology (JAMSTEC), 2-15 Natsushima, Yokosuka 237-0061, Japan (takazos@jamstec.go.jp)

[5]Dipartimento di Scienze Chimiche e Geologiche, Università degli Studi di Modena e Reggio Emilia, Via Campi 103, 41125 Modena, Italy (stefano.lugli@unimore.it)

[6]Istituto di Biologia Marina, Consorzio Universitario della Provincia di Trapani, Via Barlotta Giuseppe 4, 91100 Trapani, Italy (andrea.santulli@unipa.it)

[7]Physics and Earth Science Department, University of Parma, Parco Area delle Scienze 157/A, 43124 Parma, Italy (vinicio.manzi@unipr.it, marco.roveri@ unipr.it)

Abstract

We investigated changes in the chemical characteristics of evaporating seawater under the influence of microbial activity by conducting geochemical analyses of the brines and evaporite sediments collected from solar salterns in Trapani, Italy. The microbial activity had a substantial effect on the carbonate system parameters. Dissolved inorganic carbon (DIC) was substantially removed from the brine during the course of evaporation from the seawater to the point where calcium carbonate

precipitates, with an accompanying decrease in its carbon isotopic composition ($\delta^{13}C_{DIC}$) to as low as –10.6‰. Although the removal of DIC was due to calcium carbonate precipitation, photosynthesis, and the degassing of CO_2(aq) induced by evaporation, the presence of ^{13}C-depleted $\delta^{13}C_{DIC}$ in ponds where calcium carbonate precipitates can be attributed to the dissolution of atmospheric CO_2 because of intensive CO_2(aq) uptake by photosynthesis, and/or mineralization of organic matter by sulfate reduction. In contrast, $\delta^{13}C_{DIC}$ increased up to 7.2‰ in the salinity range where halite precipitates, which can be ascribed to the domination of the effect of degassing of CO_2(aq) under conditions with reduced microbial activity. A gradual decrease in microbial activity was also reflected in compound-specific δ^{13}C of photosynthetic pigments; isotopic fractionation associated with DIC assimilation increased linearly as the evaporation proceeded, indicating DIC-limited conditions within the microbial mats and gypsum crusts because of restricted DIC diffusion from the overlying brine and/or suppression of primary production at higher salinity.

1. INTRODUCTION

Salinity is one of the most critical environmental factors determining habitability of aquatic environment. Although salinity is potentially a strong limiting factor for

habitability, hypersaline environments are populated by a surprising diversity of microorganisms, especially in shallow settings, where benthic microbial mats form (e.g. Oren, 2002; Ley et al., 2006; Oren et al., 2009). It therefore follows that various biological processes are actively operating in the shallow hypersaline environment, strongly influencing the biogeochemical cycles and chemical characteristics of the system. In addition, seawater evaporation induces transitions in the state and composition of the microbial community through changes in various environmental factors (salinity, temperature, pH, light conditions, etc.). These changes result in modifications of the biological processes, which in turn strongly affect the environment. For these reasons, the chemical characteristics of the evaporating seawater are determined not only by physical and chemical processes induced by evaporation, but also by biological processes within the system. In this study, we focused on the solar salterns of Trapani (Sicily, Italy) to increase our understanding of the mutual interaction between physical, chemical, and biological processes with increasing salinity in hypersaline environment.

Solar salterns consist of a series of shallow ponds, normally less than 1 m deep, affording a large surface area for evaporation, with salinity increasing from seawater up to the saturation point of halite (NaCl). Different types of evaporite minerals precipitate

on the bottom of the ponds according to the degree of evaporation (Logan, 1987; Geisler-Cussey, 1997). Calcium carbonate ($CaCO_3$, calcite or aragonite) starts to precipitate in ponds in which the evaporation of the original seawater exceeds 50%. When over 80% of the original seawater has been removed by evaporation, gypsum ($CaSO_4 \cdot 2H_2O$) starts to precipitate. Benthic microbial mats usually form in the salinity range within which calcium carbonate and gypsum precipitate. Halite starts to precipitate when evaporation exceeds 90% of the original seawater. Various K-Mg salts precipitate after halite. There is no benthic microbial community in these highly evaporated ponds, but there are planktonic microorganisms in halite crystallizer ponds (e.g. Antón et al., 2000; Řeháková et al., 2009). The evaporation changes not only the chemical composition but also the physical properties of the brine: e.g., it decreases the solubility and diffusion of dissolved inorganic carbon (DIC; Raven, 1991) and changes the activity coefficients of ions through increasing ionic strength (Karcz and Zak, 1987).

One particular characteristic of these shallow hypersaline environment is the formation of a highly productive microbial mat. The hypersaline microbial mats formed at the bottom of the ponds are inhabited by highly diverse groups of microorganisms: cyanobacteria (e.g., Green et al., 2008), chemotrophic and phototrophic sulfur-oxidizing bacteria (e.g., Ollivier et al., 1994; Imhoff, 2001), and sulfate-reducing bacteria (e.g.,

91 Canfield and Des Marais, 1993; Risatti et al., 1994; Teske et al., 1998; Baumgartner et
92 al., 2006). These groups are dominant in many of the hypersaline microbial mats at
93 various sites, and together with less abundant but highly diverse groups of
94 microorganisms they form a complex community structure. This extreme diversity is
95 produced by the broad niche space provided by the light gradient and varying chemical
96 conditions within the mat, which itself is modified by biological processes of the
97 microorganisms (Ley et al., 2006).

98 Carbon, sulfur, and oxygen cycles within the mat clearly illustrate the mutual
99 interaction among the microbial communities via biological modification of the
100 chemical conditions (Van Gemerden, 1993). For example, primary production by
101 photoautotrophs generates the organic carbon that fuels the entire ecosystem, but at the
102 same time releases oxygen, which is toxic to anaerobes. The fixed carbon is degraded
103 by fermenters and mineralized to DIC by heterotrophs, sulfate-reducing bacteria and, in
104 some cases, methanogens (e.g., Van Gemerden, 1993, Orphan et al., 2008). This
105 efficient recycling of carbon inside the mat accounts in part for its high primary
106 productivity (e.g., Canfield and Des Marais, 1993; Des Marais, 2003; Kovač, 2009). On
107 the other hand, sulfide produced by sulfate reduction is toxic to aerobic microorganisms,
108 but is oxidized back to sulfate, biotically by chemotrophic and phototrophic sulfur

bacteria and abiotically by oxygen produced during photosynthesis (e.g., Revsbech et al., 1983; Fründ and Cohen, 1992; Canfield and Des Marais, 1993). The activity of these biological processes fluctuates on a daily cycle controlled by light availability (e.g., Canfield and Des Marais, 1993).

Because most hypersaline evaporative settings in natural environments harbor a microbial community, it is of critical importance to understand the responses of biological processes to increasing salinity. As described above, the physical and biological processes associated with the evaporation of seawater have the potential to affect essential elements such as carbon, nitrogen, oxygen, and sulfur. Here, we specifically focus on changes in the carbonate system, which constitutes a fundamental part of the biogeochemical cycle. The amount and chemical form of DIC, which is a resource for autotrophs, play a key role in biological processes. DIC concentrations in continental aquatic systems are maintained by water–atmosphere CO_2 exchange, precipitation and dissolution of minerals, photosynthesis, respiration, and external inputs such as soil CO_2 (e.g., Lazar and Erez, 1992). The carbon cycle in the ocean, which has the largest reservoir of DIC, also affects continental aquatic systems by controlling the atmospheric CO_2 level. There are distinct inorganic and biological controls on the carbon budget and the relative proportions of the three major dissolved

carbon forms—aqueous carbon dioxide (CO_2(aq)), bicarbonate (HCO_3^-), and carbonate ion (CO_3^{2-})—in an aquatic system. Thus, the interplay between changes in precipitating salts and microbial communities is key to understanding the changes in the carbonate system during evaporative concentration processes.

Here, we focus on the water chemistry as well as on the concentration and isotope signature of DIC in salterns, with the aim of gaining a comprehensive understanding of carbon dynamics in the shallow hypersaline environment. We also investigate changes in primary productivity along the salinity gradient by performing a compound-specific isotope analysis of photosynthetic pigments. We expect the resulting insights to also be beneficial as basic information for understanding the massive evaporation events known to have occurred repeatedly worldwide in the geological past (e.g., Hay et al., 2006; Warren, 2010).

2. MATERIALS AND METHODS

2.1. Study site

We studied three commercial solar salterns located in Trapani (Western Sicily, Italy): the Sosalt (SS), Culcasi (CU), and Chiusicella (CH) salterns (Fig. 1). These solar salterns, each consisting of multiple ponds with different salinities, differ in scale;

145 Sosalt is the largest, with a total surface area of 800 ha and an annual production of salt
146 reaching 1×10^5 tons, and Chiusicella is the smallest in both surface area (7 ha) and
147 number of ponds.

148 Progressively increasing salinities characterize each series of ponds, and the
149 corresponding evaporite minerals that precipitate at the bottom. The ponds where
150 calcium carbonate precipitates (carbonate ponds) are characterized by the formation of a
151 dense benthic microbial mat. This microbial mat consists of a slimy layer a few
152 millimeters thick, which is composed of thin yellow, green, and pink layers on the
153 surface, and black, loose deposits buried underneath (Fig. 2a, b). The gypsum ponds
154 have a thick layer of gypsum precipitates, which consists of striking stratified solid
155 layers of different colors—yellowish transparent, green, and pink layers, from the
156 surface of the precipitate to a depth averaging around 5 cm—with loose black deposits
157 below (Fig. 2c, d). Large halite crystals (Fig. 2e, f) form in the subsequent halite ponds.
158 There are apparently no benthic microbial communities in the halite ponds.

159

160 **2.2. Sampling protocols**

161 Normal seawater, brine, and deposits in the ponds were collected during the daytime
162 in September 2015 (Table 1). Seawater and brine samples were collected in 100-mL

polyacrylonitrile (PAN) bottles. Those samples collected for the measurement of total alkalinity (TA), DIC concentration, and DIC carbon isotopic composition ($\delta^{13}C_{DIC}$) were immediately poisoned with 200 μL of saturated $HgCl_2$ solution to prevent further biological activity. The lid was closed without headspace until the analysis to prevent further gas exchange with the atmosphere. The temperature and pH of brine and seawater were measured in situ using a pH meter with a combination electrode (GST-5741C; DKK-TOA Corporation, Tokyo, Japan). The effect of temperature on pH was calibrated using the equation of Gieskes (1969). The pH values are given using the seawater hydrogen ion (SWS) scale. Brine and seawater samples were kept cool in a refrigerator until analysis.

Samples of pond deposits were collected by hand or by using a hammer and chisel. Microbial mats were collected from three ponds (SS-3, CU-1, and CU-2); small gypsum crystals were found in the deposits from SS-3. Gypsum crusts were collected from three ponds (SS-1, SS-2, and CH-1), and halite crystals from two ponds (SS-4 and CU-5). Samples were stored in a freezer until analysis.

2.3. Brine and seawater sample analysis

2.3.1. Salinity

Salinity was measured by using a digital laboratory salinometer at the National Institute of Advanced Industrial Science and Technology, Japan (AIST) (Digi-Auto model 5, Tsurumi-Seiki Co., Kanagawa, Japan). Standard seawater (International Association for the Physical Sciences of the Ocean [IAPSO]) was used as a reference. Analytical precision was within ±0.01 salinity unit.

2.3.2. Ion concentrations

Brine samples were diluted on a weight basis with ultrapure water prior to analysis. Concentrations of Na^+, Mg^{2+}, and K^+ were measured by ion chromatography at the Japan Agency for Marine-Earth Science and Technology (JAMSTEC) (Dionex ICS-1600, Thermo Fisher Scientific, Inc., Waltham, Massachusetts, USA), as were Cl^-, Br^-, and SO_4^{2-} (Dionex ICS-2100, Thermo Fisher Scientific, Inc.). Elemental boron (B) and Ca^{2+} were measured using inductively coupled plasma-optical emission spectrometry at JAMSTEC (ICP-OES, SII SPS5510, SII NanoTechnology Inc., Chiba, Japan). The analytical precisions (±2σ) of replicate measurements were within ±2% for Na^+ and Cl^-, and ±10% for the other elements.

2.3.3. Total alkalinity

199 Total alkalinity was measured using a total alkalinity titrator at AIST (ATT-05,
200 Kimoto Electric Co., Osaka, Japan). Samples were titrated with 0.1 mol L^{-1} HCl, and
201 TA was calculated by the Gran method. Samples collected from CH-1, SS-4, and CU-5
202 were diluted on a weight basis with ultrapure water prior to the measurement. The
203 analytical precision of replicate measurements was within ±1.5%.
204
205 **2.3.4. DIC concentration and carbon isotopic composition**
206 For measurement of DIC, brine samples (10–50 mL) were transferred to a glass vial,
207 and the air inside was completely evacuated using a high-vacuum glass line. Next, the
208 samples were reacted with H_3PO_4 and left for 12 h so that DIC was completely
209 converted to CO_2 gas. The evolved gas was then introduced into a high-vacuum glass
210 line and separated cryogenically. The gas pressure in the glass line was recorded and
211 converted to DIC concentration. The precision of the DIC measurement was within
212 0.3%. Afterwards, the purified CO_2 gas was introduced into an isotope-ratio mass
213 spectrometer (Delta Plus XL, Thermo Fisher Scientific, Inc.) to measure the carbon
214 isotopic composition of the DIC. Isotopic compositions are expressed as conventional
215 $\delta^{13}C$ relative to Vienna Pee Dee Belemnite. The analytical precision was within 0.1‰.
216

2.4. Deposit sample analyses

2.4.1. Carbon isotopic composition of sediment TOC

Sediment samples collected from the bottom of the ponds were subsampled for measurement of $\delta^{13}C$ of organic matter ($\delta^{13}C_{TOC}$). Samples collected from the carbonate ponds were separated into two parts: the upper slimy layer and the loose black deposit underneath (Fig. 2b). The gypsum crusts were separated into four parts: the yellowish transparent, green, and pink gypsum layers, and the loose black deposits below (Fig. 2d). Subsampled deposits were freeze-dried and ground to powder. Together with ground halite samples, they were transferred to pre-cleaned smooth-wall tin capsules and treated with 0.1 mol L^{-1} HCl to remove $CaCO_3$. After the samples were dried they were analyzed for $\delta^{13}C_{TOC}$ at JAMSTEC using a modified Flash EA1112 automatic elemental analyzer connected to a Thermo Finnigan Delta plus XP isotope ratio mass spectrometer (IRMS) via a ConFlo III Interface (Ogawa et al., 2010). Isotopic compositions are expressed as conventional $\delta^{13}C$ values relative to Vienna Pee Dee Belemnite. The analytical precision was within 0.3‰.

2.4.2. Compound-specific pigment isotopic composition

The surface deposits from CU-1 and SS-3 (microbial mat), the yellowish transparent,

green, and pink layers from SS-1 and CH-1 (gypsum crust), and halite crystals from SS-4 and CU-5 were analyzed for compound-specific isotope compositions of pigments. First, the deposits were freeze-dried and ground to powder. Organic matter was extracted with acetone three times by sonication for 15 min in an ultrasonic ice bath. The acetone fraction was then extracted with *n*-hexane three times. The *n*-hexane fraction was dried completely under N_2 gas and dissolved in 100 μL of *N*,*N*-dimethylformamide for high-performance liquid chromatography (HPLC) injection. All procedures were carried out in a dark room.

Pigment isolation and purification was accomplished using dual step HPLC. The HPLC system comprised a binary pump (G1312B; Agilent, Santa Clara, California, USA), an on-line degasser (G1379B; Agilent), an autosampler (G1367C; Agilent), a column temperature controller (Cool Pocket Column Chiller; Thermo Fisher Scientific), an on-line photodiode-array detector (G4212B; Agilent), and a fraction collector (G1364C; Agilent). The pigments were isolated using an Agilent Zorbax Eclipse XDB C-18 column (4.6 mm × 250 mm; 5-μm silica particle size) with a guard column (4.6 mm × 12.5 mm; 5-μm silica particle size). The pigments were eluted isocratically with 75% acetonitrile:pyridine (100:0.5, v/v) and 25% ethyl acetate:pyridine (100:0.5, v/v) for 5 min, followed by a linear gradient of ethyl acetate:pyridine to 50% over 50 min.

253 The flow rate was set to 1 mL min^{-1} and the column temperature to 30 °C. Pigments
254 were detected by the photodiode-array detector. The structure assignment of each
255 compound was accomplished by comparing the photo-absorption spectra and the
256 retention times with those of authentic standards. Chlorophyll *a* (Chl *a*),
257 bacteriochlorophyll *a* (BChl *a*), and β-carotene were collected using the fraction
258 collector. We carefully collected the entire peak for each compound to avoid analytical
259 isotopic fractionation.

260 The collected pigments were dried completely under argon gas. Prior to the second
261 HPLC purification step, Chl *a* and BChl *a* were dissolved in 1.5 mL hexane and reacted
262 with 2 mol L^{-1} HCl to converted them to pheophytin *a* (Pheo *a*) and bacteriopheophytin
263 *a* (BPheo *a*), respectively. The hexane fraction was collected and dried completely
264 under argon gas, and dissolved in 100 μL of *N*,*N*-dimethylformamide for HPLC
265 injection. The column used for second purification step was an Agilent Zorbax Eclipse
266 PAH column (4.6 mm × 250 mm; 5-μm particle size). Pigments were eluted
267 isocratically with 80% acetonitrile:pyridine (100:0.5, v/v) and 20% ethyl
268 acetate:pyridine (100:0.5, v/v) for 5 min, followed by a linear gradient of ethyl
269 acetate:pyridine to 60% over 25 min, and a linear gradient of ethyl acetate:pyridine to
270 100% over 10 min. The flow rate was set to 1 mL min^{-1} and the column temperature to

271 15 °C.

272 The stable carbon isotopic compositions of the pigments were measured using a
273 modified EA/IRMS (Ogawa et al., 2010). Purified pigments were dissolved in
274 dichloromethane, transferred to pre-cleaned smooth-wall tin capsules, and dried before
275 analysis. The analytical precisions were within 0.3‰ for Chl *a* and BChl *a*, and 0.6‰
276 for β-carotene.

277

278 **3. RESULTS**

279 Data from the brine sample analyses are summarized in Tables 1 and S1. The brines
280 in the solar salterns originate from seawater from the same region, and precipitation of
281 evaporites is the major process occurring within the salterns. Thus, we report and
282 discuss the data from different solar salterns together, under the assumption that the
283 biological processes in the three systems are comparable. We did not determine the
284 salinity or the concentration of Na^+ and Cl^- of the brine samples collected from the
285 ponds with higher salinities (CH-1, SS-4, and CU-5) because halite crystals precipitated
286 in the sample bottles after the samples were collected.

287

288 **3.1. Variations in concentrations of inorganic elements**

The concentrations of solutes in the brines are determined mainly by condensation due to evaporation, removal by precipitation of evaporite minerals, and the effects of biological activity. One way to determine the behavior of the solutes is to normalize their concentrations by the degree of evaporation (DE; e.g., Babel and Schreiber, 2014). The DE of the brine can be estimated from the concentrations of the solutes that behave conservatively upon evaporation. In the salinity range of our samples, Mg^{2+}, K^{+}, Br^{-}, and B behave as conservative solutes. Here, we estimated the DE of each brine sample from the Mg^{2+} concentration as follows:

$$DE_{Mg} = \frac{[Mg^{2+}_{brine}]}{[Mg^{2+}_{seawater}]}$$

where $[Mg^{2+}_{seawater}]$ and $[Mg^{2+}_{brine}]$ are the molar concentrations of Mg ions in the seawater and brine samples, respectively. Normalization of the solute concentrations by DE_{Mg} cancels out the effect of condensation due to evaporation, therefore allowing the examination of the addition or removal of solutes to or from the brine.

The composition of the major ions in the sample of seawater (CU-0), which is the source of the brines in the solar salterns studied, was comparable to that reported for average modern seawater (Babel and Schreiber, 2014). The major evaporite minerals precipitated from seawater in the salinity range of our samples are calcium carbonate, gypsum, and halite. Accordingly, ions such as Ca^{2+}, HCO_3^{-}, SO_4^{2-}, Na^{+}, and Cl^{-} are

307 removed sequentially from the seawater (Fig. S1, Table S1). To evaluate the process of
308 the precipitation of evaporites in the Trapani solar salterns, we compared our results
309 with computer-modeled concentration curves, which are calculated by assuming an
310 absence of biological activity. Specifically, we compared our data with the calculations
311 of Timofeeff et al. (2001), in which the back-reaction between the brine and evaporites
312 is inhibited to simulate more realistically the evaporation process in solar salterns.
313 Major ions plotted against each other lie on the line of the modeled evaporation curves
314 (Fig. 3), indicating that, for these major ions, seawater in the solar salterns apparently
315 follows an evaporation path with no influence from biological activity.
316
317 **3.2. Variations in carbonate system parameters**
318 DIC concentrations decreased from the seawater value of 2.04 mmol L^{-1} to 1.00
319 mmol L^{-1} in the carbonate ponds, and then increased to 5.95 mmol L^{-1} in the halite
320 ponds (Fig. 4, Table 1). When normalized by DE_{Mg}, there was a sharp drop from
321 seawater to the carbonate ponds. Variations in [DIC]/DE_{Mg} were relatively small in the
322 subsequent ponds. TA increased progressively from the seawater value of 2.68 mmol
323 L^{-1} to as high as 21.1 mmol L^{-1} in the halite pond. In highly evaporated brine, a
324 substantial portion of TA originates from boric acid (Golan et al., 2016), which behaves

conservatively upon evaporation. Variations in [TA]/DE_{Mg} followed the same trend as that of [DIC]/DE_{Mg} because increases in TA due to accumulating boric acid are canceled out upon normalization. Similar variations in DIC and TA along a salinity gradient have been reported in the solar saltern of Eilat, Israel (Lazar and Erez, 1992).

Interestingly, $\delta^{13}C_{DIC}$ was highly variable during the course of evaporation (Fig. 4). It decreased substantially from the seawater value of 2.2‰ and remained low through the gypsum ponds, with a minimum of –10.6‰. There was subsequently a substantial increase in the halite ponds to the highest value of 7.2‰ (DE_{Mg} = 22.0). Lazar and Erez (1992) also reported this pattern of variation in $\delta^{13}C_{DIC}$ with increasing salinity.

Seawater pH measured at the intake of the pond system was 8.2 and increased to 8.5 in the carbonate ponds in which there was a microbial mat (Fig. 4). It then decreased gradually to reach 7.2 in the halite ponds. This characteristic pattern is commonly observed in evaporating seawater brine (Babel and Schreiber, 2014), and it has been confirmed that this pattern is not an artifact from a liquid junction error in the glass pH electrode in the concentrated solution (Sass and Ben-Yaakov, 1977). In experimentally evaporated seawater, there is a continuous decrease in pH from seawater to the point where DE_{Mg} is around 6.7 (Lazar et al., 1983). Therefore, the increase in pH that we observed up to the carbonate ponds may be due to biological processes such as CO_2(aq)

uptake for photosynthesis. Several possible mechanisms have been proposed for explaining the decrease in pH in the subsequent evaporation stages (e.g. Krumgalz, 1980; Nadler and Magaritz, 1980; McCaffrey et al., 1987).

3.3. Organic carbon isotopic composition ($\delta^{13}C_{TOC}$) of deposits

Values of $\delta^{13}C_{TOC}$ were high compared to the values in normal marine settings, and decreased from a maximum of –8.6‰ in the carbonate ponds to a minimum of –22.7‰ in the halite ponds (Fig. 5, Table S2). The differences between $\delta^{13}C_{TOC}$ and $\delta^{13}C_{DIC}$ increased as the salinity increased. Depth profiles of $\delta^{13}C_{TOC}$ do not show any common trends among ponds (Fig. 6, Table S2). The lack of a common trend may be because the isotopic signals of organisms living in the lower layers of the deposits are superimposed on the signals of upper-layer organisms, reflecting the fact that the lower-layer deposits consist of upper-layer deposits that subsequently became buried and then occupied by lower-layer dwellers. This preservation of the original mat-surface $\delta^{13}C$ signature in deeper layers has been reported previously (e.g., Des Marais et al., 1992).

3.4. Distribution of pigments and their carbon isotopic composition

The distribution of pigments was similar for the same types of samples from different

361 solar salterns. Therefore, only representative chromatograms are shown: from the
362 surface slimy layer of the microbial mats in the carbonate ponds, from the yellowish
363 transparent, green, and pink layers of the gypsum crusts in the gypsum ponds, and from
364 the halite crystals in the halite ponds (Fig. S2).

365 The major pigments detected in the surface slimy layer of the carbonate ponds were
366 the Chl *a* series, the BChl *a* series, and various carotenoids. The Chl *a* series includes
367 Chl *a* and its degradation products, Pheo *a* and pyropheophytin *a* (PPheo *a*). The BChl *a*
368 series includes BChl *a* and its degradation products, BPheo *a* and
369 bacteriopyropheophytin *a* (BPPheo *a*). Among the various carotenoids detected, the
370 peaks with a retention time around 23 min were identified as β-carotene and its
371 degradation products (β-carotene series), based on a comparison with the authentic
372 standard. The relative concentrations of the original pigments (i.e., Chl *a* and BChl *a*)
373 were substantially higher than their counterpart degradation products. We measured the
374 $\delta^{13}C$ of Chl *a*, BChl *a*, and β-carotene.

375 In the gypsum crust, the main pigments in the yellowish transparent layer and the
376 green layer were the Chl *a* series and smaller peaks of carotenoids, including the
377 β-carotene series. The pink layer contained Chl *a*, BChl *a*, and the β-carotene series,
378 with BChl *a* highest in concentration. The Chl *a* in the pink layer was probably

originally from the cyanobacteria or algae in the upper yellowish and green layers, because they migrate upward as the photic and oxic zones moves upward with the growth of the gypsum crust. We therefore measured $\delta^{13}C$ of Chl *a* in the yellowish transparent layer and the green layer, which is dominated by cyanobacteria and algae, and BChl *a* in the pink layer dominated by purple sulfur bacteria. We also measured $\delta^{13}C$ of β-carotene in the yellowish transparent layer of the gypsum crust.

The pigment distribution in the halite crystals from the halite ponds was completely different from that in the carbonate and gypsum ponds, with the β-carotene series in highest concentrations and extremely low Chl *a* concentrations. Because there was not enough Chl *a* for isotopic measurement, we determined $\delta^{13}C$ of only the β-carotene series in halite samples.

The depth variations of pigment $\delta^{13}C$ values showed similar patterns in all ponds: $\delta^{13}C$ of BChl *a* was lower than that of Chl *a* in both microbial mats and gypsum crusts (Fig. 6, Table 2). In a comparison between ponds, the $\delta^{13}C$ values of Chl *a*, BChl *a*, and β-carotene were highest in CU-1, at –11.5‰, –19.5‰ and –22.1‰, respectively (Fig. 5). The $\delta^{13}C$ values of all pigments showed decreasing trends as evaporation proceeded, and reached minimum values of –20.6‰ and –26.3‰ in CH-1 for Chl *a* and BChl *a*, respectively, and –28.5‰ in CU-5 for β-carotene. The $\delta^{13}C_{TOC}$ of the surface sediment

397 samples showed similar trends.

398 We calculated an isotopic fractionation factor from the $\delta^{13}C_{DIC}$ in the surface brine
399 and that of TOC, Chl *a*, and β-carotene: $\varepsilon \equiv (R_{org}/R_{DIC}) \times 1000$ (‰), where R_{org} is
400 $^{13}C/^{12}C$ for TOC, Chl *a*, or β-carotene. We specifically used the $\delta^{13}C$ of Chl *a* and
401 β-carotene originating from the surface slimy layer of the microbial mats, the yellowish
402 transparent layer from the gypsum crusts, and the halite crystals, which contain
403 pigments derived from microorganisms assumed to assimilate DIC mainly from the
404 surface brine. Overall, the values of ε were lower in the lower salinity ponds, and
405 increased more or less linearly as evaporation proceeds (Fig. 5). Between TOC, Chl *a*,
406 and β-carotene, ε of β-carotene was highest, ranging from 14.9‰ to 36.0‰, followed by
407 that of Chl *a*, ranging between 6.4‰ and 17.3‰, and the lowest, that of TOC, ranging
408 from 3.5‰ to 30.2‰.

409 We did not quantify the concentration of each pigment because of the somewhat
410 patchy distribution of the colored layers on the pond bottoms. However, our rough
411 estimates indicate that the concentrations of Chl *a* and BChl *a* were on the order of
412 micrograms per gram of dry sediment for the microbial mat and the gypsum crust.

413

414 **4. DISCUSSION**

4.1. Changes in primary production with increasing salinity

For estimating the primary productivity, the $\delta^{13}C$ of pigments has an advantage over $\delta^{13}C_{TOC}$ because the pigments derive exclusively from photoautotrophs; thus, other factors such as heterotrophic activity, which potentially affects $\delta^{13}C_{TOC}$, are excluded. Compound-specific isotope analysis of chlorophylls has been successfully used to improve understanding of modern and past biogeochemical cycles, especially in the euphotic zone (e.g., Sachs and Repeta, 1999; Ohkouchi et al., 2005; Kusch et al., 2010; Tyler et al., 2010; Isaji et al., 2015).

Among the pigments measured in this study, Chl *a* and β-carotene are synthesized by aerobic photoautotrophs such as cyanobacteria and algae, and BChl *a* is produced by the purple sulfur bacteria present in the pink layer of the microbial mat. In solar salterns, both planktonic and benthic cyanobacteria and algae are generally present. In Spain, the reported concentrations of Chl *a* in the brine of a solar saltern were around 2–15 μg L^{-1} (Joint et al., 2002). On the other hand, the concentrations of Chl *a* in the benthic deposits of the Trapani solar salterns were on the order of micrograms per gram of dry sediment, which is much higher than the concentration of the overlying brine reported in Joint et al. (2002). Although we did not measure the concentration of Chl *a* in the brine in this study, we speculate that the dominant primary producer is the benthic

community in ponds where benthic microbial mat is formed. Chl *a* and β-carotene in the halite ponds probably originate from planktonic photoautotrophs, because these ponds contain no benthic microbial mat. Specifically, *Dunaliella salina* is the likely candidate, because this organism is known to be a dominant primary producer in halite ponds (e.g., Řeháková et al., 2009), and it also accumulates high amounts of β-carotene (Oren, 2005).

There are several possible factors that could account for the lower $\delta^{13}C$ of BChl *a* compared to that of Chl *a* in the benthic community (Fig. 6). One is the difference in the source of DIC utilized by each photoautotroph. Because the purple sulfur bacteria inhabit the deeper layer of the mat, some proportion of DIC assimilated by them is supplied through mineralization of the organic matter within the mat. The values of $\delta^{13}C_{TOC}$ indicate that $\delta^{13}C$ of the mineralized DIC is lower than that of DIC in the surface brine, because isotopic fractionation associated with degradation of organic matter is negligible (e.g., Meyers and Eadie, 1993). Another factor is the chemical species of DIC assimilated by the photoautotroph. Cyanobacteria are capable of assimilating HCO_3^- through active transport (e.g., Kaplan et al., 1980; Badger and Price, 2003). Because HCO_3^- is enriched in ^{13}C compared to CO_2(aq) by 8.4‰ under the temperature of 30 °C (Mook et al., 1974), active assimilation of HCO_3^- by

451 cyanobacteria may have resulted in the relatively high $\delta^{13}C$ of Chl *a*. As for the purple
452 sulfur bacteria, $\delta^{13}C$ depletion in BChl *a* compared to Chl *a* has been reported from the
453 saline meromictic Lake Kaiike in Japan (Ohkouchi et al., 2005). Because purple sulfur
454 bacteria, cyanobacteria, and algae use identical biochemical pathways for carbon
455 assimilation and chlorophyll biosynthesis, differences in their $\delta^{13}C$ can be ascribed to
456 physiological factors such as growth rate, cell size, or geometry (Pancost et al., 1997;
457 Popp et al., 1998; Bidigare et al., 1999; Ohkouchi et al., 2008).

458 The isotopic fractionation factor (ε) calculated from Chl *a* and β-carotene increased
459 almost linearly with increasing salinity (Fig. 5). Because the source photoautotrophs of
460 these pigments do not change substantially along the salinity gradient (i.e.,
461 cyanobacteria and/or algae), there are several possible explanations for this observation.
462 The habitat of the photoautotrophs is one of the major factors controlling ε along the
463 salinity gradient, because while planktonic photoautotrophs such as *D. salina* inhabiting
464 the halite ponds can utilize DIC in the surface brine, benthic cyanobacteria and algae in
465 the microbial mats and gypsum crusts utilize DIC that diffuses from the overlying brine.
466 DIC diffusion into the benthic microbial mat can be limited by a diffusive boundary
467 layer over the mat surface (Jørgensen, 1994b) or within the mat (Wieland et al., 2001).
468 As for the gypsum crust, there is likely only limited exchange of brine through the pore

469 water. These limits on diffusion could result in DIC-limited conditions inside the
470 microbial mat, which is expressed as a relatively small ε without depletion of DIC in the
471 overlying brine. Indeed, limited DIC diffusion into the microbial mat has also been
472 considered as a possible reason for relatively high $\delta^{13}C_{TOC}$ and therefore low values of ε
473 (e.g., Des Marais and Canfield, 1994; Schouten et al., 2001). From this perspective, the
474 relatively large ε in the halite ponds is because the habitat of the dominant
475 photoautotroph, *D. salina*, is in the surface brine, where conditions are not DIC-limited.
476 Another possible factor controlling ε along the salinity gradient comes from the
477 observation that ε increases when compared among ponds of the same type: the
478 carbonate ponds (CU-1, SS-3), the gypsum ponds (SS-1, CH-1), and the halite ponds
479 (SS-4, CU-5). The only exception is the decrease in ε calculated from $\delta^{13}C$ of β-carotene
480 in the carbonate ponds. If the diffusion rate of DIC into the mat or the crust does not
481 change substantially with increasing salinity, then the increase in ε can be interpreted as
482 reflecting a lower proportion of DIC assimilated by photoautotrophs under the higher
483 salinities. In other words, increasing salinity may have suppressed primary production.
484 This suggestion is consistent with the findings of previous studies that photosynthesis
485 decreases with increasing salinity (Oren, 2009) in microbial mats (e.g., Pinckney et al.,
486 1995; Wieland and Kühl, 2006) and gypsum crusts (e.g., Caumette et al., 1994, Canfield

et al., 2004), as well as in the planktonic community of halite ponds (Joint et al., 2002). Salinity may directly control the primary productivity by affecting the physiology of photoautotrophs, or indirectly by affecting the elemental cycles of nutrients such as nitrogen, phosphorus, and iron.

4.2. Effect of biological activities on the chemical evolution of evaporating seawater

4.2.1. Influence of sulfate reduction on brine

One of the highest rates of sulfate reduction known occurs in hypersaline microbial mats (Canfield and Des Marais, 1991). Sulfate reduction removes SO_4^{2-} from brine by reduction to H_2S or HS^- and subsequent precipitation as various metal sulfides (e.g., Wieland et al., 2005; Valdivieso-Ojeda et al., 2014). Although this process must have removed some portion of SO_4^{2-} from the brine in this study, concentrations of SO_4^{2-} plotted against other major ions lie on the line of the ideal curve (Fig. 3). To evaluate the influence of the sulfate reduction in the brine, we roughly estimated the amount of sulfate removed on the basis of sulfate reduction rates in hypersaline microbial mats and gypsum crusts of the solar salterns of Guerrero Negro, Mexico (Canfield and Des Marais, 1991, 1993), Eilat, Israel (Fründ and Cohen, 1992; Jørgensen, 1994a; Canfield et al., 2004; Sørensen et al., 2004), and Salins-de-Giraud, France (Caumette et al., 1994).

505 Assuming an average pond water depth of 50 cm, we calculated the amount of SO_4^{2-}
506 reduced by 20 cm^2 of the mat, which corresponds to 1 L of overlying brine. The
507 calculated value varied substantially for both the microbial mats and the gypsum crusts;
508 both varied between tens of micromoles to millimoles per liter per day. In contrast, the
509 SO_4^{2-} in the overlying brine in the Trapani solar salterns ranged from 79.2 to 233.2
510 mmol L^{-1} from the carbonate to the gypsum ponds.

511 Although sulfate reduction rates were not measured in the Trapani solar salterns, this
512 rough estimation implies that sulfate reduction can influence the SO_4^{2-} concentration of
513 the brine if the reduction is on the order of millimoles per liter per day. The fact that the
514 SO_4^{2-} concentration tracks the ideal evaporation curve therefore indicates that SO_4^{2-} is
515 supplied by other processes to compensate any loss through reduction, or that the sulfate
516 reduction rate in the Trapani solar salterns is low. One possible source of SO_4^{2-} for the
517 former explanation is oxidation of the reduced sulfur species by chemotrophic and
518 phototrophic sulfur bacteria or by oxygen produced by photosynthesis in the upper layer
519 of deposits and surface brine (e.g., Revsbech et al., 1983; Fründ and Cohen, 1992;
520 Canfield and Des Marais, 1993). Note that decreases in SO_4^{2-} and increases in total
521 alkalinity (TA) are canceled out by sulfide oxidation, but increases in DIC are not.

522

4.2.2. Effect of biological processes on the brine carbonate system

In the shallow hypersaline environment where benthic microbial mats form, carbonate system parameters, i.e., DIC, TA, pH, and pCO_2, are affected by various processes such as calcium carbonate precipitation and dissolution (equation 1 below), photosynthesis and respiration (Eq. 2), sulfate reduction (Eq. 3), sulfide oxidation (Eq. 4), and CO_2(g) exchange with the atmosphere. The following equations describe these processes.

$$Ca^{2+} + 2HCO_3^- \rightleftarrows CaCO_3(s) + CO_2(g) + H_2O \quad (1)$$

$$106CO_2 + 16HNO_3 + H_3PO_4 + 122H_2O \rightleftarrows (CH_2O)_{106}(NH_3)_{16}(H_3PO_4) + 138O_2 \quad (2)$$

$$SO_4^{2-} + 2CH_2O \rightarrow HS^- + 2HCO_3^- + H^+ \quad (3)$$

$$HS^- + 2O_2 \rightarrow SO_4^{2-} + H^+ \quad (4)$$

Our values for $[DIC]/DE_{Mg}$ and $[TA]/DE_{Mg}$ indicate that DIC and TA are removed from the brine during the course of evaporation from the seawater to the carbonate ponds, accompanied by a substantial drop in $\delta^{13}C_{DIC}$ (Fig. 4). In this salinity range, calcium carbonate precipitation is one of the major process affecting DIC concentrations, decreasing the $\delta^{13}C_{DIC}$ of the brine by preferentially removing ^{13}C from

DIC reservoirs. The typical enrichment factors for carbon isotope fractionation between calcium carbonate and DIC are +1.0‰ and +2.7‰ for calcite and aragonite, respectively (Romanek et al., 1992). Theoretically, the decrease in $\delta^{13}C_{DIC}$ in CU-1 from the seawater value of 2.2‰ to –5.1‰ could be reached if almost all DIC precipitated as calcium carbonate. However, calcium carbonate precipitation from seawater to DE_{Mg} = 6.7 results in a TA loss of around 60% of the source seawater, in the absence of biological activity (Lazar et al., 1983). Therefore, calcium carbonate precipitation alone cannot explain the drop in $\delta^{13}C_{DIC}$ from 2.2‰ to –5.1‰ (from seawater to CU-1) or from –5.1‰ to –10.6‰ (from CU-1 to CU-2).

Whereas DIC is affected by processes such as calcium carbonate precipitation and dissolution, photosynthesis and respiration, sulfate reduction, and CO_2(g) exchange with the atmosphere, TA is primarily affected by precipitation and dissolution of calcium carbonate, sulfate reduction, and sulfide oxidation. We suggested in section 4.2.1 that the loss of SO_4^{2-} through sulfate reduction was compensated for by sulfide oxidation, or that the rate of sulfate reduction was low. These observations implies that the net change in TA must have also been near zero. Cyanobacteria, the main photoautotroph in the hypersaline microbial mat, are capable of assimilating HCO_3^- during photosynthesis (e.g., Kaplan et al., 1980; Badger and Price, 2003). This process does not affect TA,

559 however, because they release OH^- when utilizing HCO_3^- as the carbon source (e.g.,
560 Prins and Elzenga, 1989).

561 On the basis of these observations, we calculated the amount of calcium carbonate
562 precipitated from the changes in TA, taking the transition from CU-0 (seawater) to
563 CU-1 (DE = 2.7) as the model case. It is calculated that 1.40 mmol L^{-1} of TA is lost
564 from the seawater to CU-1. According to Eq. (1), the precipitation of one mole of
565 calcium carbonate utilizes two moles of HCO_3^- and releases one mole of CO_2(g). The
566 buffering effect of seawater reduces the actual amount of CO_2(g) liberated to the
567 atmosphere to around 0.6 mole per mole of calcium carbonate precipitated (Ware et al.,
568 1992; Frankignoulle et al., 1994). Under the assumption that this rule is applicable to
569 the hypersaline solutions in saltern ponds, 1.40 mmol L^{-1} of TA loss is equivalent to the
570 precipitation of 0.70 mmol L^{-1} calcium carbonate and production of 0.70 mmol L^{-1} of
571 CO_2(g), of which 0.28 mmol L^{-1} is re-dissolved into the solution, during the transition
572 from seawater to the brine in CU-1. This results in a decrease of 1.12 mmol L^{-1} of DIC,
573 because calcium carbonate precipitation decreases DIC and TA equally but the
574 re-dissolution of CO_2(g) increases only DIC. However, the actual decrease in DIC from
575 CU-0 to CU-1 was 1.57 mmol L^{-1}, according to the changes from seawater to CU-1.
576 This value indicates that 0.45 mmol L^{-1} of DIC was lost by processes other than

577 calcium carbonate precipitation (Fig. 7).

578 There are several possible processes responsible for the loss of DIC other than
579 calcium carbonate precipitation. One is carbon fixation by photoautotrophs, which
580 preferentially removes ^{13}C-depleted DIC from the brine. The isotopic fractionation
581 factor (ε) calculated from the $\delta^{13}C$ of pigments indicates that photosynthesis was more
582 active in the lower salinity ponds (Fig. 5). The degassing of CO_2(aq) due to a decrease
583 in solubility induced by evaporation also removes ^{13}C-depleted DIC from the brine (Li
584 and Tsui, 1971; Stiller et al., 1985; Raven, 1991; Barkan et al., 2001). This process was
585 active throughout the evaporation path. Thus, although these processes that remove
586 ^{13}C-depleted DIC from the brine could balance the DIC budget, there must be other
587 processes supplying ^{13}C-depleted DIC to explain the ^{13}C-depleted $\delta^{13}C_{DIC}$ of the
588 carbonate ponds. We propose several processes that may account for the supply of
589 ^{13}C-depleted DIC:

590 (1) Because intensive photosynthesis and degassing due to evaporation remove
591 CO_2(aq) from the brine, some DIC must have been supplied by equilibrium with
592 atmospheric CO_2, which is relatively depleted in ^{13}C (e.g. Keeling, 1958).
593 Moreover, Baertschi (1952) suggested that ^{13}C-depleted CO_2 might be selectively
594 dissolved into brine from the atmosphere under alkaline conditions (“the Baertschi

595 effect"). As also suggested by Lazar and Erez (1992), this process may be
596 responsible for the ^{13}C-depleted DIC in the brine of the carbonate ponds.
597 (2) A previous study excluded sulfate reduction releasing DIC in the form of HCO_3^-
598 as the main cause of relatively low $\delta^{13}C_{DIC}$ of the brine because there was no
599 substantial increase in [TA]/DE_{Mg} with increasing DE_{Mg} (Fig. 4; Lazer and Erez,
600 1992). In the Trapani solar salterns, the changes in SO_4^{2-} concentration suggest
601 that the loss of SO_4^{2-} through sulfate reduction was compensated for by sulfide
602 oxidation, or else the rate of sulfate reduction was low (Fig. 3). As suggested in
603 section 4.2.1, sulfate reduction coupled with sulfide oxidation cancels out
604 increases in TA, but not DIC. Therefore, we cannot exclude the possibility that the
605 ^{13}C-depleted DIC was supplied by sulfate reduction. It may originate from the
606 benthic microbial mat within the pond, or from the highly productive microbial
607 communities in less evaporated, upstream ponds (Joint et al., 2002). Note that the
608 actual amount of DIC that diffuses into the overlying brine is less than the amount
609 mineralized from organic matter, because of restricted diffusion of DIC within the
610 mat (Wieland et al., 2001) and on the mat surface (Jørgensen, 1994b). Indeed,
611 Canfield and Des Marais (1993) suggested that a large proportion of mineralized
612 DIC is fixed back into organic matter within the mat during the day, whereas it

613 diffuses into the overlying brine at night.

614 In the gypsum and halite ponds, $\delta^{13}C_{DIC}$ gradually increased to reach 7.2‰ in CU-5.
615 This increase indicates that the biological processes that reduced the $\delta^{13}C_{DIC}$ of the
616 carbonate and gypsum ponds are suppressed in the halite ponds, and that $\delta^{13}C_{DIC}$ is
617 primarily controlled by the degassing of CO_2(aq) (Stiller et al., 1985). A reduced
618 influence of biological activity on $\delta^{13}C_{DIC}$ is consistent with the discussion about the
619 $\delta^{13}C$ of pigments indicating that photosynthesis is more active in the lower salinity
620 ponds.

621 Another observation is that DIC concentrations and TA in CH-1 and CU-5 were
622 higher than those found in the solar saltern of Eilat, Israel (Lazar and Erez, 1992). These
623 higher concentrations might be because the biological processes that potentially
624 accumulate DIC and TA were more intense in the upper-stream, lower salinity ponds of
625 the Trapani solar salterns. Indeed, as in CU-5, DIC and TA in the upstream ponds (CU-1
626 and CU-2) were also slightly higher than the values reported by Lazar and Erez (1992),
627 suggesting that biological processes in the lower salinity ponds accumulated in and
628 modified the chemical composition of higher salinity ponds. Alternatively, the higher
629 DIC and TA in the Trapani ponds may be due to dissolution of calcium carbonate
630 supplied by aerial transport, because experimentally evaporated seawater is known to be

631 undersaturated with respect to aragonite (Lazar et al., 1983).

632

633 **5. CONCLUSIONS AND IMPLICATIONS**

634 In this study, we demonstrated that the isotopic fractionation factor (ε) calculated
635 from $\delta^{13}C$ of chlorophyll *a* and β-carotene, which originate from cyanobacteria and
636 algae, increased linearly along an increasing salinity gradient in solar saltern ponds in
637 Trapani, Italy. We ascribe this observation to the DIC-limited conditions within the
638 microbial mats and gypsum crusts caused by restricted DIC diffusion from the overlying
639 brine, and/or suppression of primary production with increasing salinity. Variations in
640 the carbonate system parameters also indicate changing microbial activity along the
641 salinity gradient. We propose that dissolution of atmospheric CO_2 into the brine through
642 intensive CO_2(aq) uptake by photosynthesis and mineralization of organic matter by
643 sulfate reduction may be the processes responsible for ^{13}C-depleted DIC in the
644 carbonate and gypsum ponds. In contrast, we attribute increases in $\delta^{13}C_{DIC}$ in
645 subsequent ponds to the dominance of degassing of CO_2(aq) with reduced microbial
646 activity.

647 One important reason for elucidating the carbon cycle of hypersaline environments is
648 that such environments may have had a substantial impact on the global carbon cycle

649 during massive evaporation events that repeatedly occurred worldwide in the geological
650 past (e.g., Hay et al., 2006; Warren, 2010). This study and previous studies (e.g., Stiller
651 et al., 1985; Lazar and Erez, 1992) have demonstrated that CO_2 exchange between brine
652 and the atmosphere is an important factor controlling the brine carbonate system during
653 the evaporation of seawater. There is still some debate about the environmental setting
654 (e.g., shallow vs. deep) and the extent of evaporation (e.g., total desiccation vs.
655 non-desiccation) of the massive evaporation events in the past (e.g., the Messinian
656 Salinity Crisis; Hsü et al., 1973; Roveri et al., 2014). However, further constraints on
657 the evaporation model during these events, as well as the elucidation of the behavior of
658 the carbonate system under various evaporative settings, will enhance our understanding
659 of the role of hypersaline environments in the global carbon cycle.
660
661 **Acknowledgements**
662 We are grateful to SoSalt Spa and R.N.O Saline di Trapani e Paceco for permission to
663 sample Trapani solar works. We gratefully acknowledge Dr. Kana Nagashima of the
664 Japan Agency for Marine-Earth Science and Technology (JAMSTEC) for assistance in
665 X-ray diffraction analysis. We also thank Dr. R. H. Byrne, an associate editor, Dr. B.
666 Lazar, and two anonymous reviewers for their insightful comments. This study was

667 partly supported by a Japan Society for the Promotion of Science (JSPS) Research
668 Fellowship (16J07844) to Y. Isaji, Grants-in-Aid to H. Kawahata (Nos. 19340146,
669 22224009, and 15H02139), and JAMSTEC. All data used in this article are available
670 from the corresponding author.

671

672 **References**

673 Antón J., Rosselló-Mora R., Rodríguez-Valera F., and Amann R. (2000) Extremely
674 halophilic bacteria in crystallizer ponds from solar saltern. *Appl. Environ. Microbiol.*
675 **66**, 3052–3057.

676 Babel M., and Schreiber B. C. (2014) Geochemistry of evaporites and evolution of
677 seawater. In *Treatise on geochemistry, 2nd edn.* (eds. H. Holland and K. Turekian).
678 Elsevier, Oxford. pp. 483–560.

679 Badger M. R., and Price G. D. (2003) CO_2 concentrating mechanisms in cyanobacteria:
680 molecular components, their diversity and evolution. *J. Exp. Bot.* **54**, 609–622.

681 Baertschi P. (1952) Die Fraktionierung der Kohlenstoffisotopen bei der absorption von
682 Kohlendioxyd. *Helv. Chim. Acta* **35**, 1030–1036.

683 Barkan E., Luz B., and Lazar B. (2001) Dynamics of the carbon dioxide system in the
684 Dead Sea. *Geochim. Cosmochim. Acta* **65**, 355–368.

685 Baumgartner L. K., Reid R. P., Dupraz C., Decho A. W., Buckley D. H., Spear J. R.,
686 Przekop K.M., and Visscher P. T. (2006) Sulfate reducing bacteria in microbial mats:
687 changing paradigms, new discoveries. *Sediment. Geol.* **185**, 131–145.
688 Bidigare R. R., Hanson K. L., Buessler K. O., Wakeham S. G., Freeman K. H., Pancost
689 R. D., Millero F. J., Steinberg P., Popp B. N., Latasa M., Landry M. R., and Laws E.
690 A. (1999) Iron-stimulated changes in ^{13}C fractionation and export by equatorial
691 Pacific phytoplankton: toward a paleogrowth rate proxy. *Paleoceanography* **14**,
692 589–595.
693 Canfield D. E., and Des Marais D. J. (1991) Aerobic sulfate reduction in microbial mats.
694 *Science* **251**, 1471–1473.
695 Canfield D. E., and Des Marais D. J. (1993) Biogeochemical cycles of carbon, sulfur,
696 and free oxygen in a microbial mat. *Geochim. Cosmochim. Acta* **57**, 3971–3984.
697 Canfield D. E., Sørensen K. B., and Oren A. (2004) Biogeochemistry of a
698 gypsum-encrusted microbial ecosystem. *Geobiology* **2**, 133–150.
699 Caumette P., Matheron R., Raymond N., and Relexans J. C. (1994) Microbial mats in
700 the hypersaline ponds of Mediterranean salterns (Salins-de-Giraud, France). *FEMS*
701 *Microbiol. Ecol.* **13**, 273–286.
702 Des Marais D. J. (2003) Biogeochemistry of hypersaline microbial mats illustrates the

703 dynamics of modern microbial ecosystems and the early evolution of the biosphere.
704 *Biol. Bull.* **204**, 160–167.
705 Des Marais D. J., and Canfield D. E. (1994) The carbon isotope biogeochemistry of
706 microbial mats. In *Microbial Mats: Structure, Development and Environmental*
707 *Significance* (eds. Stal L. J. and Caumette P.). Springer, Berlin. NATO ASI Series G,
708 Vol. 35, pp. 289–298.
709 Des Marais D. J., Bauld J., Palmisano A. C., Summons R. E., and Ward D. M. (1992)
710 The biogeochemistry of carbon in modern microbial mats. In *The proterozoic*
711 *biosphere: a multidisciplinary study* (eds. Schopf J. W. and Klein C.). Cambridge
712 University Press, Cambridge, pp. 299–308.
713 Frankignoulle M., Canon C., and Gattuso J. P. (1994) Marine calcification as a source of
714 carbon dioxide: Positive feedback of increasing atmospheric CO_2. *Limnol. Oceanogr.*
715 **39**, 458–462.
716 Fründ C., and Cohen Y. (1992) Diurnal cycles of sulfate reduction under oxic conditions
717 in cyanobacterial mats. *Appl. Environ. Microbiol.* **58**, 70–77.
718 Geisler-Cussey D. (1997) Modern depositional facies developed in evaporative
719 environments (marine, mixed, and nonmarine). In *Sedimentary Deposition in Rift and*
720 *Foreland Basins in France and Spain (Paleogene and Lower Neogene)* (eds. Busson

721 G. and Schreiber B. C.). Columbia University Press, New York. pp. 3–42.
722 Gieskes J. M. (1969). Effect of temperature on the pH of seawater. *Limnol. Oceanogr.*
723 **14**, 679–685.
724 Golan R., Gavrieli I., Ganor J., and Lazar, B. (2016) Controls on the pH of hyper-saline
725 lakes-A lesson from the Dead Sea. *Earth Planet. Sci. Lett.* **434**, 289–297.
726 Green S. J., Blackford C., Bucki P., Jahnke L. L., and Prufert-Bebout L. (2008) A
727 salinity and sulfate manipulation of hypersaline microbial mats reveals stasis in the
728 cyanobacterial community structure. *The ISME journal*, **2**, 457–470.
729 Hay W. W., Migdisov A., Balukhovsky A. N., Wold C. N., Flögel S., and Söding E.
730 (2006) Evaporites and the salinity of the ocean during the Phanerozoic: implications
731 for climate, ocean circulation and life. *Palaeogeogr. Palaeoclimatol. Palaeoecol.* **240**,
732 3–46.
733 Hsü K. J., Ryan W. B. F., and Cita M. B. (1973) Late Miocene desiccation of the
734 Mediterranean. *Nature*, **242**, 240–244.
735 Imhoff J. F. (2001) True marine and halophilic anoxygenic phototrophic bacteria. *Arch.*
736 *Microbiol.* **176**, 243–254.
737 Isaji Y., Kawahata H., Ohkouchi N., Ogawa N. O., Murayama M., Inoue K., and Tamaki
738 K. (2015) Varying responses to Indian monsoons during the past 220 kyr recorded in

739 deep- sea sediments in inner and outer regions of the Gulf of Aden. *J. Geophys. Res.*
740 *Oceans.* **120**, 7253–7270.
741 Joint I., Henriksen P., Garde K., and Riemann B. (2002) Primary production, nutrient
742 assimilation and microzooplankton grazing along a hypersaline gradient. *FEMS*
743 *Microbiol. Ecol.* **39**, 245–257.
744 Jørgensen B. B. (1994a) Sulfate reduction and thiosulfate transformations in a
745 cyanobacterial mat during a diel oxygen cycle. *FEMS Microbiol. Ecol.* **13**, 303–312.
746 Jørgensen B. B. (1994b) Diffusion processes and boundary layers in microbial mats. In
747 *Microbial Mats: Structure, Development and Environmental Significance* (eds. Stal L.
748 J. and Caumette P.). Springer, Berlin. NATO ASI Series G, Vol. 35, pp. 243–253.
749 Kaplan A., Badger M. R., and Berry J. A. (1980) Photosynthesis and the intracellular
750 inorganic carbon pool in the bluegreen alga *Anabaena variabilis*: response to external
751 CO_2 concentration. *Planta* **149**, 219–226.
752 Karcz I., and Zak I. (1987) Bedforms in salt deposits of the Dead Sea brines. *J.*
753 *Sediment. Petrol.* **57**, 723–735.
754 Keeling C. D. (1958) The concentration and isotopic abundances of atmospheric carbon
755 dioxide in rural areas. *Geochim. Cosmochim. Acta* **13**, 322–334.
756 Kovač N., (2009) Chemical characterization of stromatolitic “Petola” layer (Sečovlje

757 Salt-Pans, Slovenia) using FT-IR spectroscopy. *Annales. Ser. Hist. Nat.* **19**, 95–102.

758 Krumgalz B. S. (1980) Salt effect on the pH of hypersaline solutions. In: *Hypersaline*
759 *Brines and Evaporitic Environments. Developments in Sedimentology, vol. 28* (eds,
760 Nissenbaum A.). Elsevier, Amsterdam. pp. 73–83.

761 Kusch S., Kashiyama Y., Ogawa N. O., Altabet M., Butzin M., Friedrich J., Ohkouchi
762 N., and Mollenhauer G. (2010) Implications for chloro- and pheopigment synthesis
763 and preservation from combined compound-specific $\delta^{13}C$, $\delta^{15}N$, and $\Delta^{14}C$ analysis,
764 *Biogeosci. Discuss.* **7**, 6265–6294.

765 Lazar B., and Erez J. (1992) Carbon geochemistry of marine-derived brines: I. ^{13}C
766 depletions due to intense photosynthesis. *Geochim. Cosmochim. Acta* **56**, 335–345.

767 Lazar, B., Starinsky A., Katz A., Sass E., and Ben- Yaakov S. (1983) The carbonate
768 system in hypersaline solutions: alkalinity and $CaCO_3$ solubility of evaporated
769 seawater. *Limnol. Oceanogr.* **28**, 978–986.

770 Ley R. E., Harris J. K., Wilcox J., Spear J. R., Miller S. R., Bebout B. M., Maresca J. A.,
771 Bryant D. A., Sogin M L. and Pace N. R. (2006) Unexpected diversity and
772 complexity of the Guerrero Negro hypersaline microbial mat. *Appl. Environ.*
773 *Microbiol.* **72**, 3685–3695.

774 Li Y. H., and Tsui T. F. (1971) The solubility of CO_2 in water and sea water. *J. Geophys.*

Res. **76**, 4203–4207.

Logan B. W. (1987) The MacLeod evaporite basin, western Australia. Holocene environments, sediments and geological evolution. *AAPG Memoir* **44**, 1–140.

McCaffrey M. A., Lazar B., and Holland H. D. (1987) The evaporation path of seawater and the coprecipitation of Br^- and K^+ with halite. *J. Sediment. Petrol.* **57,** 928–937.

Meyers P. A., and Eadie B. J. (1993) Sources, degradation and recycling of organic matter associated with sinking particles in Lake Michigan. *Org. Geochem.* **20**, 47–56.

Mook W. G., Bommerson J. C., and Staverman W. H. (1974) Carbon isotope fractionation between dissolved bicarbonate and gaseous carbon dioxide. *Earth Planet. Sci. Lett.* **22**, 169–176.

Nadler A., and Magaritz M. (1980) Studies of marine solution basins - Isotopic and compositional changes during evaporation. In: *Hypersaline Brines and Evaporitic Environments. Developments in Sedimentology, vol. 28* (eds, Nissenbaum A.). Elsevier, Amsterdam. pp. 115–129.

Ogawa N. O., Nagata T., Kitazato H., and Ohkouchi N. (2010) Ultra sensitive elemental analyzer/isotope ratio mass spectrometer for stable nitrogen and carbon isotope analyses. In *Earth, Life, and Isotopes* (eds. Ohkouchi N., Tayasu I., and Koba K.). Kyoto University Press, Kyoto. pp. 339–353.

793 Ohkouchi N., Nakajima Y., Okada H., Ogawa N. O., Suga H., Oguri K., and Kitazato H.
794 (2005) Biogeochemical processes in the saline meromictic Lake Kaiike, Japan:
795 implications from molecular isotopic evidences of photosynthetic pigments. *Environ.*
796 *Microbiol.* **7**, 1009–1016.
797 Ohkouchi N., Nakajima Y., Ogawa N. O., Chikaraishi Y., Suga H., Sakai S., and
798 Kitazato H. (2008) Carbon isotopic composition of the tetrapyrrole nucleus in
799 chloropigments from a saline meromictic lake: A mechanistic view for interpreting
800 the isotopic signature of alkyl porphyrins in geological samples. *Org. Geochem.* **39**,
801 521–531.
802 Ollivier B., Caumette P., Garcia J. L., and Mah R. A. (1994) Anaerobic bacteria from
803 hypersaline environments. *Microbiol. Mol. Biol. Rev.* ***58***, 27–38.
804 Oren A. (2002) Diversity of halophilic microorganisms: environments, phylogeny,
805 physiology, and applications. *J. Ind. Microbiol. Biotechnol.* **28**, 56–63.
806 Oren A. (2005) A hundred years of Dunaliella research: 1905–2005. *Saline systems*, *1*,
807 1.
808 Oren A. (2009) Saltern evaporation ponds as model systems for the study of primary
809 production processes under hypersaline conditions. *Aquat. Microb. Ecol.* **56**,
810 193–204.

811 Oren A., Sørensen K.B., Canfield D.E., Teske A.P., Ionescu D. Lipski A. and Altendorf
812 K. (2009) Microbial communities and processes within a hypersaline gypsum crust in
813 a saltern evaporation pond (Eilat, Israel). *Hydrobiologia* **626**,15–26.
814 Orphan V. J., Jahnke L. L., Embaye T., Turk K. A., Pernthaler A., Summons R. E., and
815 Des Marais D. J. (2008) Characterization and spatial distribution of methanogens and
816 methanogenic biosignatures in hypersaline microbial mats of Baja California.
817 *Geobiology* **6**, 376–393.
818 Pancost R. D., Freeman K. H., Wakeham S. G., and Robertson C. Y. (1997) Controls on
819 carbon isotope fractionation by diatoms in the Peru upwelling region. *Geochim.*
820 *Cosmochim. Acta* **61**, 4983‑4991.
821 Pinckney J., Paerl H. W., and Bebout B. M. (1995) Salinity control of benthic microbial
822 mat community production in a Bahamian hypersaline lagoon. *J. Exp. Mar. Biol. Ecol.*
823 **187**, 223–237.
824 Popp B. N., Laws E. A., Bidigare R. R., Dore J. E., Hanson K. L., and Wakeham S. G.
825 (1998) Effect of phytoplankton cell geometry on carbon isotope fractionation.
826 *Geochim. Cosmochim. Acta* **62**, 69‑77.
827 Prins H. B. A., and Elzenga, J. T. M. (1989) Bicarbonate utilization: function and
828 mechanism. *Aqua. Bot.* **34**, 59–83.

829 Raven J. A. (1991) Implications of inorganic carbon utilization: ecology, evolution, and
830 geochemistry. *Can. J. Bot*. **69**, 908–924.
831 Řeháková K., Zapomělová E., Prášil O., Veselá J., Medová H., and Oren A. (2009)
832 Composition changes of phototrophic microbial communities along the salinity
833 gradient in the solar saltern evaporation ponds of Eilat, Israel. *Hydrobiologia* **636**,
834 77–88.
835 Revsbech N. P., Jørgensen B. B., Blackburn T. H., and Cohen Y. (1983) Microelectrode
836 studies of the photosynthesis and O_2, H_2S, and pH profiles of a microbial mat. *Limnol.*
837 *Oceanogr.* **28**, 1062–1074.
838 Risatti J. B., Capman W. C., and Stahl D. A. (1994) Community structure of a microbial
839 mat: the phylogenetic dimension. *Proc. Natl. Acad. Sci. USA* **91**, 10173–10177.
840 Romanek C., Grossman E. and Morse J. (1992) Carbon isotopic fractionation in
841 synthetic calcite, effects of temperature and precipitation rate. *Geochim. Cosmochim.*
842 *Acta* **56**, 419–430.
843 Roveri M., Flecker R., Krijgsman W., Lofi J., Lugli S., Manzi V., Sierro F. J., Bertini A.,
844 Camerlenghi A., De Lange G., Govers R., Hilgen F. J., Hübscher C., Meijer P., and
845 Stoica M. (2014) The Messinian Salinity Crisis: Past and future of a great challenge
846 for marine sciences. *Mar. Geol.* **352**, 25–58.

847 Sachs J. P., and Repeta D. J. (1999) Oligotrophy and nitrogen fixation during eastern
848 Mediterranean sapropel events. *Science* **286**, 2485–2488.
849 Sass E., and Ben-Yaakov S. (1977) The carbonate system in hypersaline solutions: Dead
850 Sea brines. *Mar. Chem.* **5**, 183–199.
851 Schouten S., Hartgers W. A., Lòpez J. F., Grimalt J. O., and Damsté J. S. S. (2001) A
852 molecular isotopic study of ^{13}C-enriched organic matter in evaporitic deposits:
853 recognition of CO_2-limited ecosystems. *Org. Geochem.* **32**, 277–286.
854 Sørensen K. B., Canfield D. E., and Oren A. (2004) Salinity responses of benthic
855 microbial communities in a solar saltern (Eilat, Israel). *Appl. Environ. Microbiol.* **70**,
856 1608–1616.
857 Stiller M., Rounick J. S., and Shasha S. (1985) Extreme carbon-isotope enrichments in
858 evaporating brines. *Nature* **316**, 434–435.
859 Teske A., Ramsing N. B., Habicht K., Fukui M., Küver J., Jørgensen B. B., and Cohen Y.
860 (1998) Sulfate-reducing bacteria and their activities in cyanobacterial mats of Solar
861 Lake (Sinai, Egypt). *Appl. Environ. Microbiol.* **64**, 2943–2951.
862 Timofeeff, M. N., Lowenstein T. K., Brennan S. T., Demicco R. V., Zimmermann H.,
863 Horita J., and Von Borstel L. E. (2001) Evaluating seawater chemistry from fluid
864 inclusions in halite: examples from modern marine and nonmarine environments.

865 *Geochim. Cosmochim. Acta* **65**, 2293–2300.

866 Tyler J., Kashiyama Y., Ohkouchi N., Ogawa N. O., Yokoyama Y., Chikaraishi Y., Staff
867 R. A., Ikehara M., Ramsey C. B., Bryant C., Brock F., Gotanda K., Haraguchi T.,
868 Yonenobu H., and Nakagawa T. (2010) Tracking aquatic change using
869 chlorine-specific carbon and nitrogen isotopes: The last glacial-interglacial transition
870 at Lake Suigetsu, Japan, *Geochem. Geophys. Geosyst.* **11**, Q09010.

871 Valdivieso-Ojeda J. A., Huerta-Diaz M. A., and Delgadillo-Hinojosa F. (2014) High
872 enrichment of molybdenum in hypersaline microbial mats of Guerrero Negro, Baja
873 California Sur, Mexico. *Chem. Geol.* **363**, 341–354.

874 Van Gemerden H. (1993) Microbial mats: a joint venture. *Mar. Geol.* **113**, 3–25.

875 Ware J. R., Smith S. V., and Reaka-Kudla M. L. (1992) Coral reefs: sources or sinks of
876 atmospheric CO_2?. *Coral reefs, 11*(3), 127–130.

877 Warren J. K. (2010) Evaporites through time: Tectonic, climatic and eustatic controls in
878 marine and nonmarine deposits. *Earth-Sci. Rev.* **98**, 217–268.

879 Wieland A., and Kühl M. (2006) Regulation of photosynthesis and oxygen consumption
880 in a hypersaline cyanobacterial mat (Camargue, France) by irradiance, temperature
881 and salinity. *FEMS Microbiol. Ecol.* **55**, 195–210.

882 Wieland A., de Beer D., Damgaard L. R., Kuhl M., Van Dusschoten D., and Van As H.

(2001) Fine-scale measurement of diffusivity in a microbial mat with nuclear magnetic resonance imaging. *Limnol. Oceanogr.* **46**, 248–259.

Wieland A., Zopfi J., Benthien M., and Kühl M. (2005) Biogeochemistry of an iron-rich hypersaline microbial mat (Camargue, France). *Microb. Ecol.* **49**, 34–49.

Figure captions

Fig. 1. Locations of the solar salterns investigated in this study. The aerial image is from Google Earth.

Fig. 2. Photographs showing the appearance of the ponds and the bottom deposits. (a) carbonate pond; (b) bottom deposit of carbonate pond showing a slimy layer a few millimeters thick, which is composed of thin yellow, green, and pink layers on the surface, and black, loose deposits buried underneath; (c) gypsum pond; (d) gypsum crust from gypsum pond showing yellowish transparent, green, and pink layers, from the surface, and loose black deposits below; (e) halite pond; (f) halite crystals from halite pond.

Fig. 3. Cross plots of the major ions of the Trapani brines (blue circles) along with the computer-modeled evaporation path of modern seawater (solid lines; Timofeeff et al., 2001). Plotted for comparison are brine data from the Inagua crystallizer ponds (Bahamas) analyzed by McCaffrey et al. (1987) (blank triangles).

Fig. 4. Variations in dissolved inorganic carbon (DIC) concentrations, total alkalinity

(TA), $\delta^{13}C_{DIC}$, and pH (blue circles), and DIC and TA normalized to the degree of evaporation calculated from magnesium concentrations (DE_{Mg}; red circles). The bars at the top of the figure show the precipitation ranges for calcium carbonate, gypsum, and halite.

Fig. 5. Variations in $\delta^{13}C$ of dissolved inorganic carbon (DIC, blue stars), total organic carbon (TOC, gray circles), chlorophyll *a* (green circles), and β-carotene (red circles), as well as the fractionation factor ε calculated from $\delta^{13}C$ of TOC and pigments.

Fig. 6. Depth profiles of $\delta^{13}C$ of chlorophyll *a* (Chl *a*) originating from cyanobacteria and/or algae (green circles), bacteriochlorophyll *a* (BChl *a*) from purple sulfur bacteria (red circles), and total organic carbon (TOC, gray squares) in the microbial mats of the carbonate ponds (CU-1 and SS-3) and the gypsum crusts of the gypsum ponds (SS-1 and CH-1). Blue circles indicate the $\delta^{13}C$ of dissolved inorganic carbon (DIC) in the surface brine. CU, Culcasi; SS, Sosalt; CH, Chiusicella

Fig. 7. (a) Cross plot of dissolved inorganic carbon (DIC) concentrations and total alkalinity (TA) normalized to the degree of evaporation based on magnesium ion

concentrations ([DIC]/DE_{Mg} and [TA]/DE_{Mg}, respectively). Dotted black arrows A and B indicate changes due to utilization of HCO_3^- and re-dissolution of CO_2(g) by calcium carbonate precipitation during the transition from seawater (CU-0) to the carbonate pond (CU-1, DE_{Mg} = 2.7), respectively. Dotted red arrow C indicates the supply of DIC necessary to explain [DIC]/DE_{Mg} and [TA]/DE_{Mg} in CU-1. Solid arrows in the bottom right corner indicate the direction and slope of the following processes: (1) calcium carbonate precipitation, (2) photosynthesis and respiration, (3) sulfate reduction, (4) sulfide oxidation, (5) dissolution of atmospheric CO_2, and (6) degassing of CO_2(aq). (b) Close-up view of (a). Numbers next to the symbols are DE_{Mg} values. CU, Culcasi.

Tables

Table 1. Concentration of dissolved inorganic carbon (DIC) and its carbon isotopic composition ($\delta^{13}C_{DIC}$), total alkalinity (TA), and pH of seawater and brine from the Culcasi (CU), Sosalt (SS), and Chiusicella (CH) solar salterns in Trapani, Sicily, Italy. Numbers in the sample names refer to individual ponds at the salterns. SWS, seawater pH scale.

Sample	Type of evaporite	DIC (mmol L^{-1})	TA (mmol L^{-1})	$\delta^{13}C_{DIC}$ (‰)	pH (SWS)
CU-0	Seawater	2.04	2.68	2.2	8.2
CU-1	Carbonate	1.25	3.40	–5.0	8.5
CU-2	Carbonate	1.25	4.03	–10.6	8.5
SS-3	Carbonate	1.00	3.85	–8.6	8.3
SS-1	Gypsum	1.09	4.22	–8.2	8.2
SS-2	Gypsum	1.31	4.73	–9.9	8.0
CH-1	Gypsum	4.38	11.90	–3.2	7.5
SS-4	Halite	3.06	9.24	–5.2	7.3
CU-5	Halite	5.95	21.10	7.2	7.0

Table 2. $\delta^{13}C$ of chlorophyll *a* (Chl *a*), bacteriochlorophyll *a* (BChl *a*), and β-carotene extracted from deposits collected from the Culcasi (CU), Sosalt (SS), and Chiusicella (CH) solar salterns in Trapani, Sicily, Italy. Numbers in the sample names refer to individual ponds at the salterns. Analytical errors are based on replicate measurements of standard material.

Sample	Type of evaporite	Layer	Compound	$\delta^{13}C$ (‰)	Error (2σ)
CU-1-1	Carbonate	Top slimy	Chl *a*	–11.5	0.23
			BChl *a*	–19.7	0.23
			β-carotene	–22.1	0.39
SS-3-1			Chl *a*	–20.1	0.15
			BChl *a*	–23.4	0.15
			β-carotene	–23.7	0.39
SS-1-1	Gypsum	Yellowish	Chl *a*	–17.9	0.23
			β-carotene	–25.9	0.37
SS-1-2		Green	Chl *a*	–17.0	0.23
SS-1-3		Pink	BChl *a*	–20.6	0.23
CH-1-1		Yellowish	Chl *a*	–20.6	0.15
			β-carotene	–23.6	0.57
CH-1-2		Green	Chl *a*	–18.6	0.23
CH-1-3		Pink	BChl *a*	–26.3	0.23
SS-4	Halite	Bulk crystal	β-carotene	–25.8	0.15
CU-5			β-carotene	–28.5	0.37

Figure 1

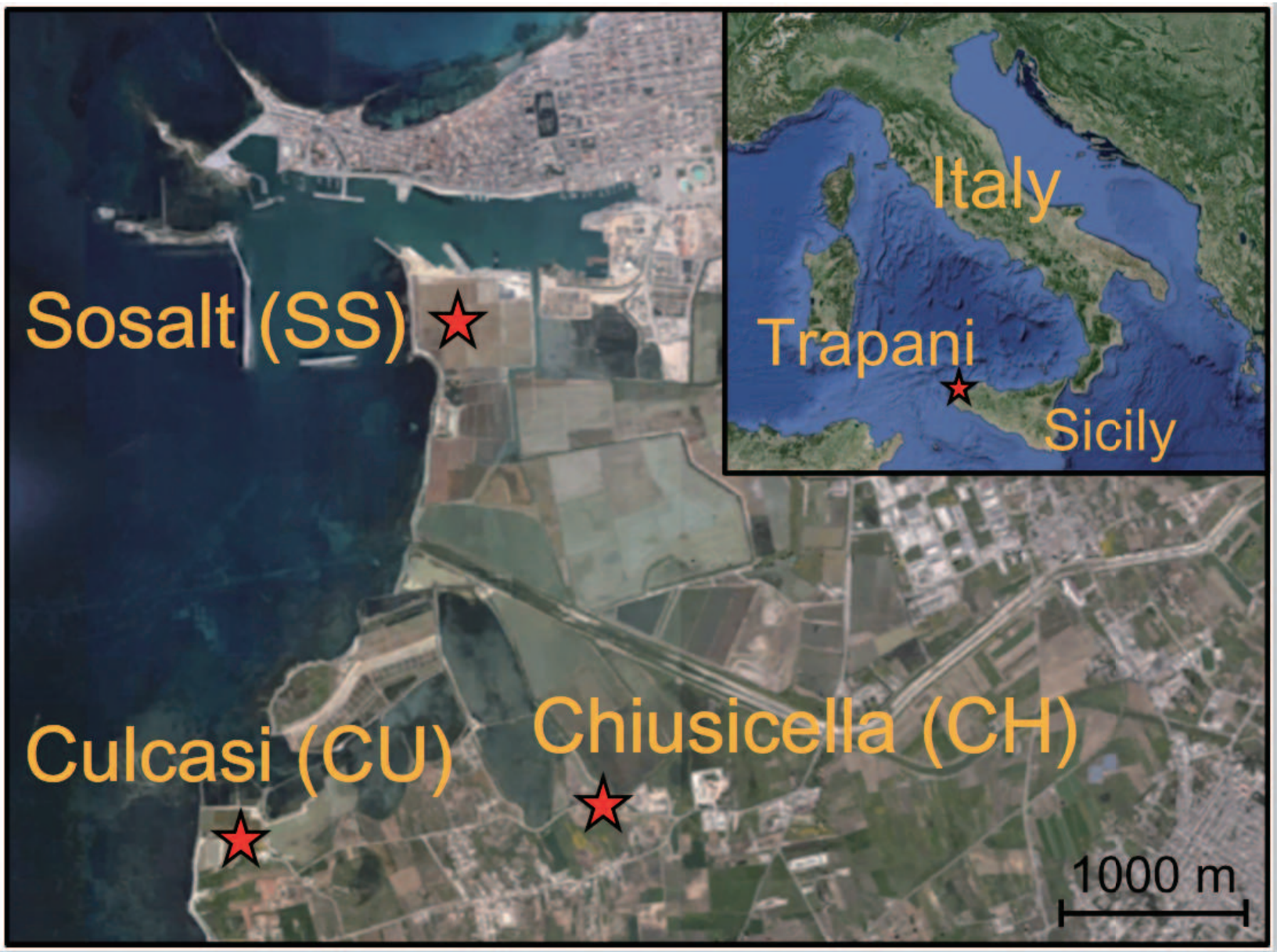

Italy
Trapani
Sicily
Sosalt (SS)
Culcasi (CU)
Chiusicella (CH)
1000 m

Figure 2

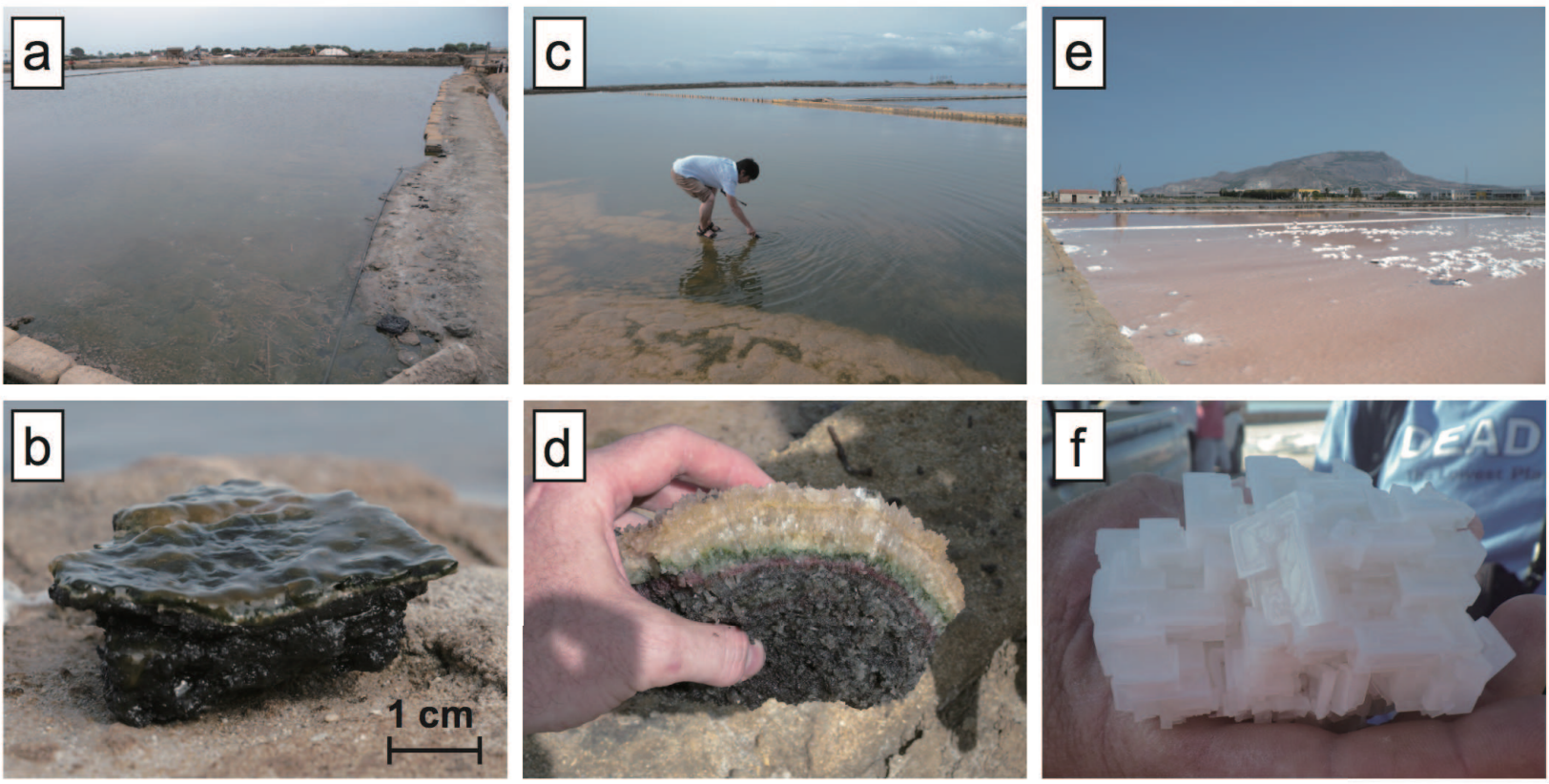
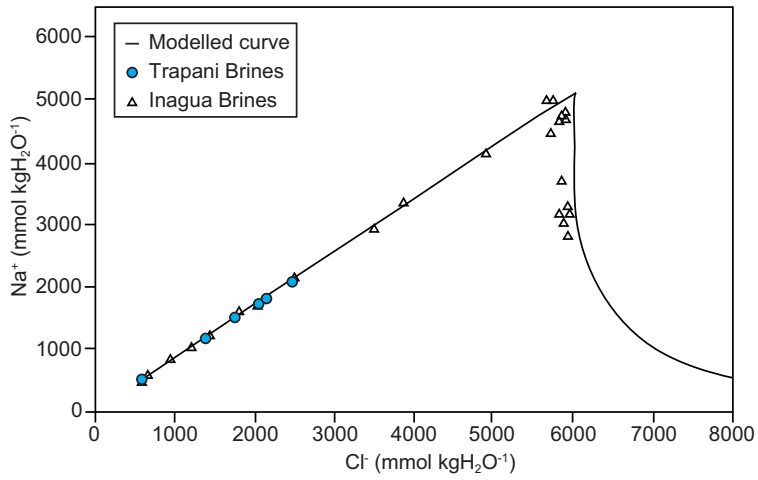
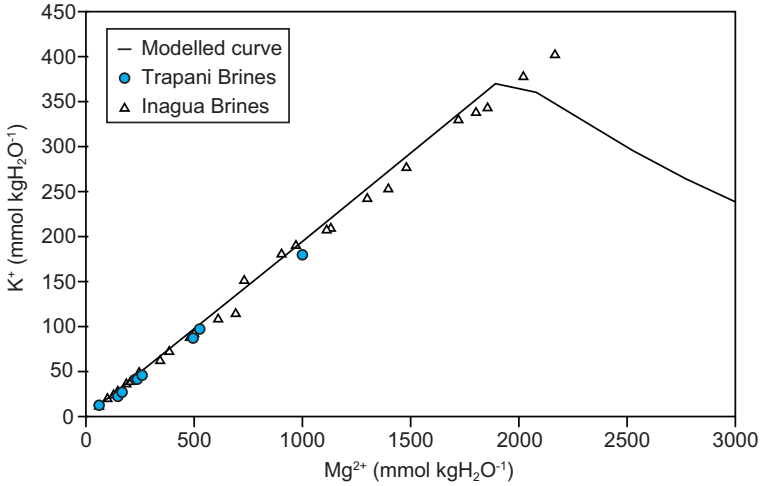
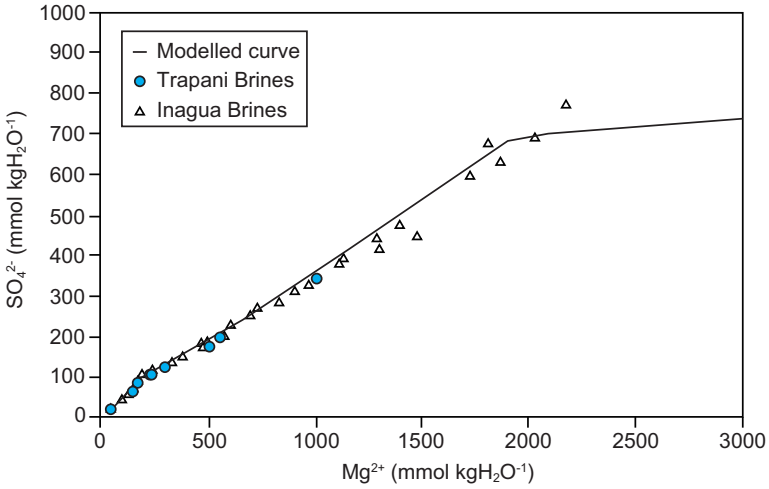


Figure 3


Modelled curve
Trapani Brines
Inagua Brines
Na+ (mmol kgH2O-1)
Cl- (mmol kgH2O-1)
0
1000
2000
3000
4000
5000
6000
7000
8000


Modelled curve
Trapani Brines
Inagua Brines
K+ (mmol kgH2O-1)
Mg2+ (mmol kgH2O-1)
0
50
100
150
200
250
300
350
400
450
500
1000
1500
2000
2500
3000


Modelled curve
Trapani Brines
Inagua Brines
SO4 2- (mmol kgH2O-1)
Mg2+ (mmol kgH2O-1)
0
100
200
300
400
500
600
700
800
900
1000
1500
2000
2500
3000

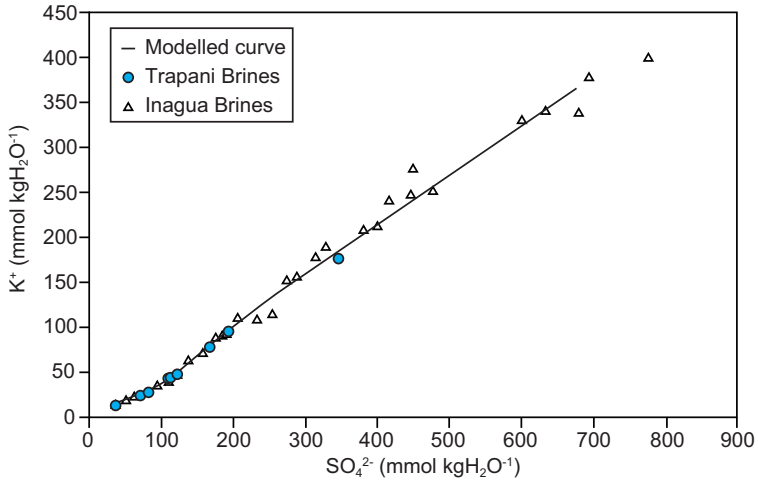

Modelled curve
Trapani Brines
Inagua Brines
K+ (mmol kgH2O-1)
SO4 2- (mmol kgH2O-1)
0
50
100
150
200
250
300
350
400
450
500
600
700
800
900

Figure 4

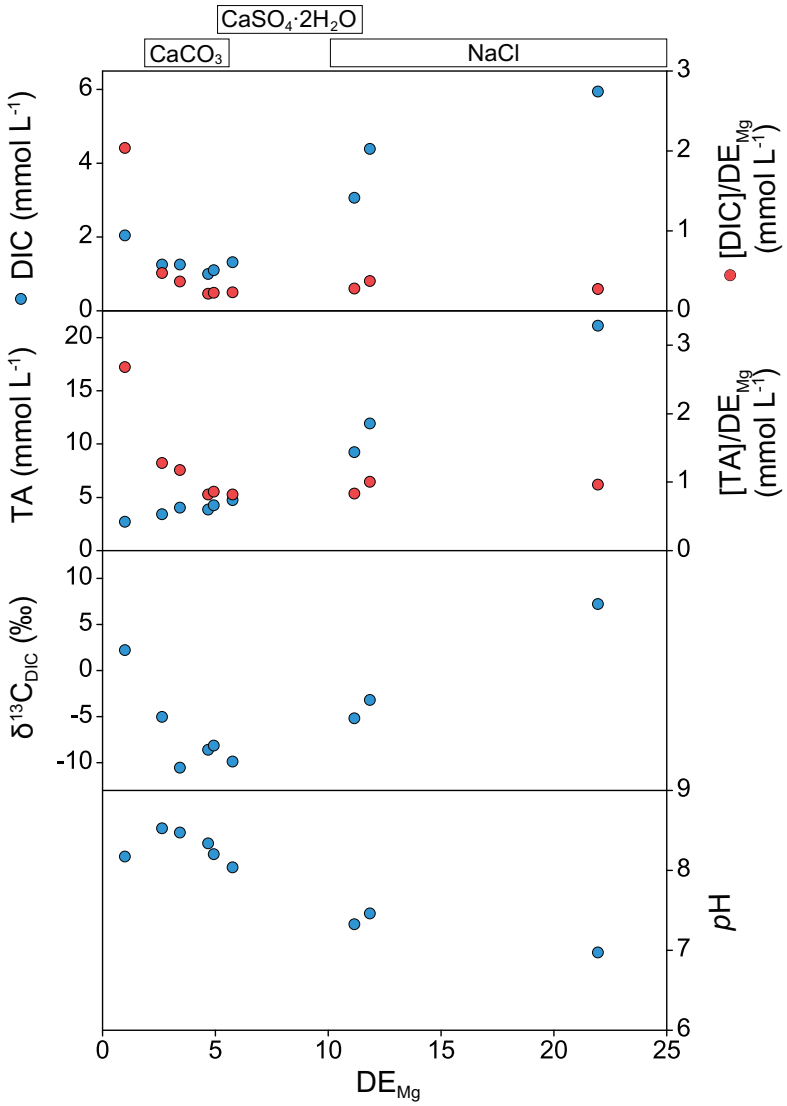

CaSO4·2H2O
CaCO3
NaCl
DIC (mmol L-1)
[DIC]/DEMg (mmol L-1)
TA (mmol L-1)
[TA]/DEMg (mmol L-1)
δ13CDIC (‰)
pH
DEMg

Figure 5

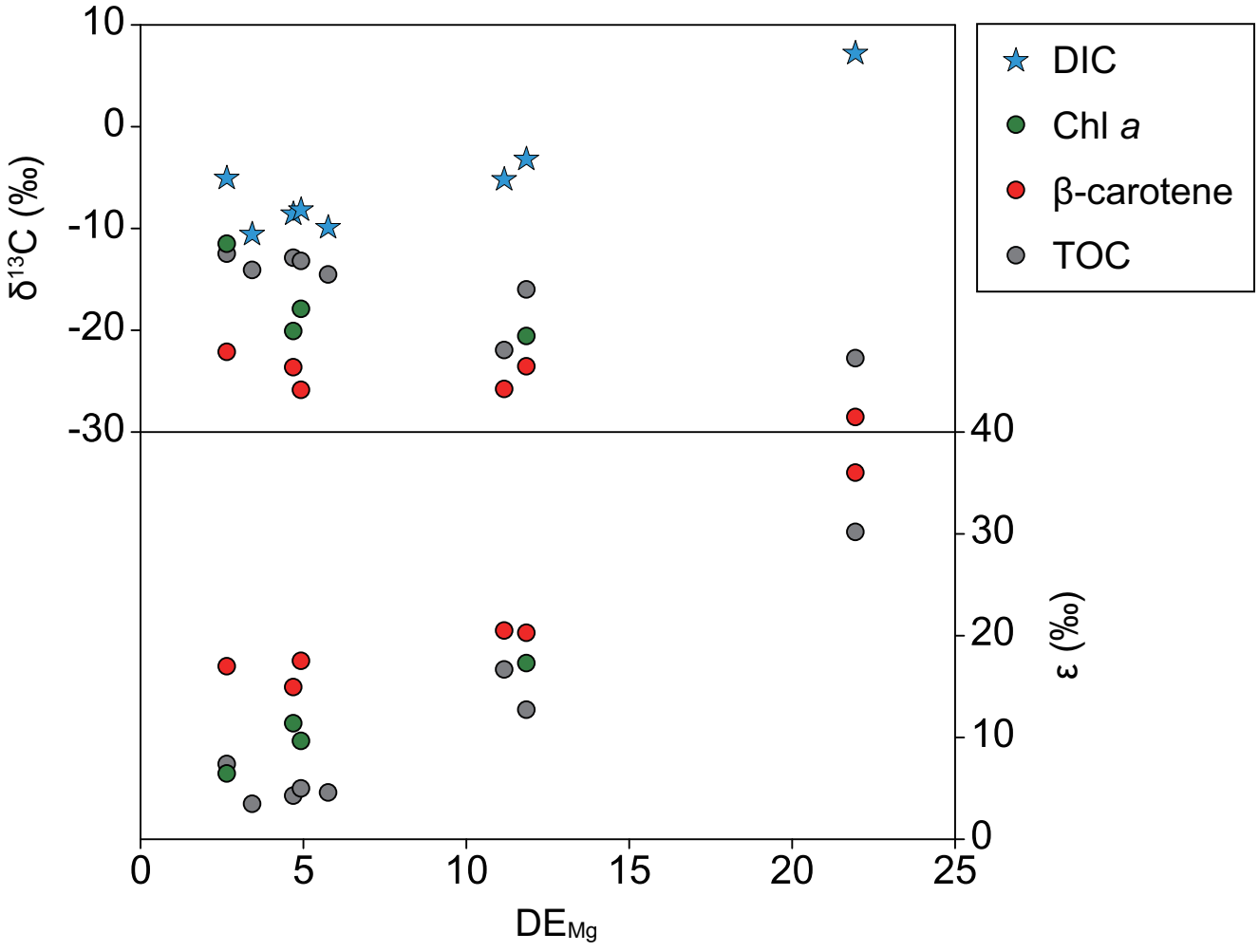

10
0
-10
-20
-30
δ13C (‰)
40
30
20
10
0
ε (‰)
0
5
10
15
20
25
DEMg
DIC
Chl a
β-carotene
TOC

Figure 6

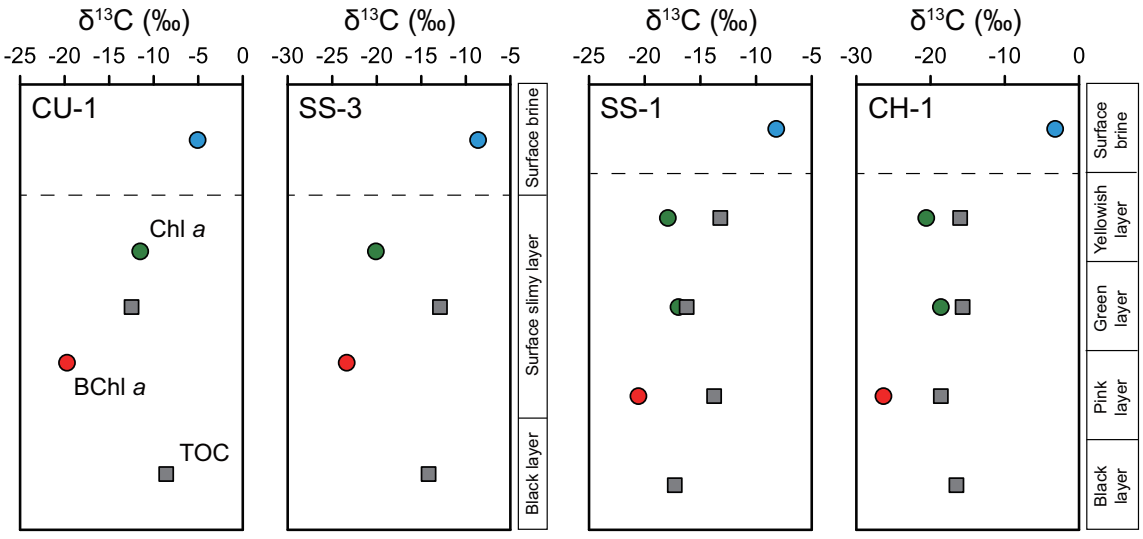
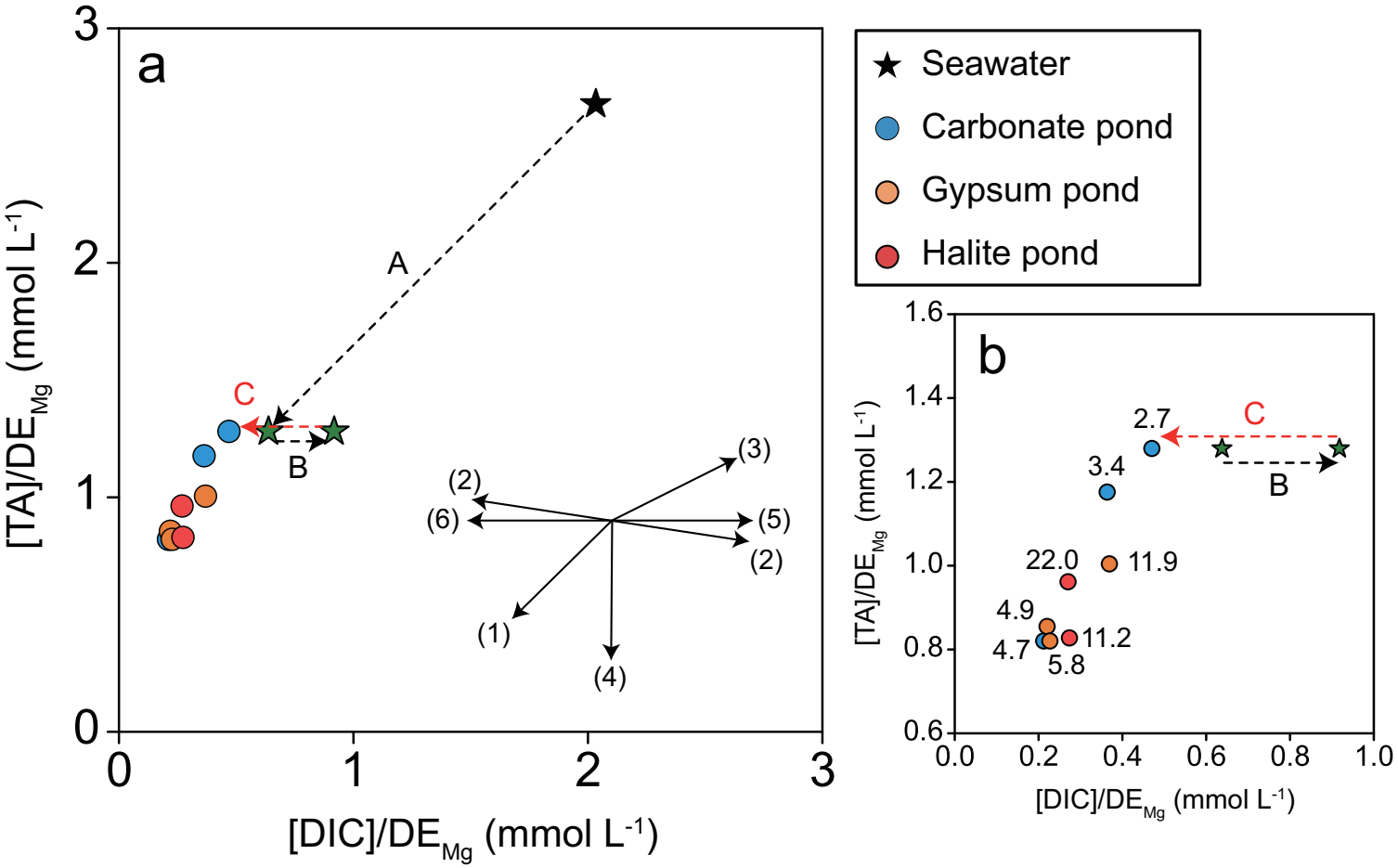

δ13C (‰)
-25 -20 -15 -10 -5 0
CU-1
Chl a
BChl a
TOC
δ13C (‰)
-30 -25 -20 -15 -10 -5
SS-3
δ13C (‰)
-25 -20 -15 -10 -5
SS-1
δ13C (‰)
-30 -20 -10 0
CH-1
Surface brine
Surface slimy layer
Black layer
Surface brine
Yellowish layer
Green layer
Pink layer
Black layer

Figure 7


a
b
Seawater
Carbonate pond
Gypsum pond
Halite pond
A
B
C
(1)
(2)
(3)
(4)
(5)
(6)
2.7
3.4
22.0
11.9
4.9
4.7
11.2
5.8
[TA]/DE$_{Mg}$ (mmol L^{-1})
[DIC]/DE$_{Mg}$ (mmol L^{-1})